Evidence for orthorhombic distortion in the ordered state of $ZnCr_2O_4$: A magnetic resonance study

V. N. Glazkov,[1] A. M. Farutin,[1] V. Tsurkan,[2,3] H.-A. Krug von Nidda,[2] and A. Loidl[2]
[1]*P. L. Kapitza Institute for Physical Problems, RAS, 119334 Moscow, Russia*
[2]*Experimental Physics V, Center for Electronic Correlations and Magnetism, University of Augsburg, 86135 Augsburg, Germany*
[3]*Institute of Applied Physics, Academy of Science of Moldova, MD-2028 Chişinău, Republic of Moldova*
(Received 3 July 2008; revised manuscript received 30 December 2008; published 30 January 2009)

We present an elaborate electron-spin-resonance study of the low-energy dynamics and magnetization in the ordered phase of the magnetically frustrated spinel $ZnCr_2O_4$. We observed several resonance modes corresponding to different structural domains and found that the number of domains can be easily reduced by field cooling the sample through the transition point. To describe the observed antiferromagnetic resonance spectra, it is necessary to take into account an orthorhombic lattice distortion in addition to the earlier reported tetragonal distortion which both appear at the antiferromagnetic phase transition.

DOI: 10.1103/PhysRevB.79.024431 PACS number(s): 75.25.+z, 75.50.Ee, 76.50.+g

I. INTRODUCTION

The intriguing physics of spinel compounds is the focus of current solid-state research. The current hot debates on the origin of exotic phenomena and ground states in magnetic spinels concern, e.g., the Verwey transition in Fe_3O_4,[1,2] heavy-fermion formation in LiV_2O_4,[3,4] colossal magnetoresistance in Cu-doped $FeCr_2S_4$,[5,6] gigantic Kerr rotation[7] and the orbital glass state in $FeCr_2S_4$,[8] the spin-orbital liquid in $FeSc_2S_4$,[9] the colossal magnetocapacitive effect in $CdCr_2S_4$ and $HgCr_2S_4$,[10,11] the negative thermal expansion and strong spin-phonon coupling in $ZnCr_2Se_4$ and $ZnCr_2S_4$,[12–14] the spin dimerization in $CuIr_2S_4$ (Ref. 15) and $MgTi_2O_4$,[16] and the spin-Peierls-type transitions in three-dimensional solids.[17–19] The appearance of these fascinating ground states is attributed to the competition of charge, spin, and orbital degrees of freedom, which are strongly coupled to the lattice.

Additional complexity in the normal AB_2X_4 spinels arises from the frustration effects related to the topological constrains of the pyrochlore lattice of corner-sharing tetrahedra of the *B*-site magnetic ions. In this geometry, the exchange interaction alone cannot select a unique ground state. As a result, the magnetic system remains in the disordered state down to temperatures much lower than the scale provided by the exchange interaction. In $ZnCr_2O_4$ strong direct antiferromagnetic (AFM) Cr-Cr exchange is manifested by the Curie-Weiss temperature of about −400 K, while magnetic order appears around 12 K via a first-order phase transition. At this transition the aforementioned degeneracy is lifted by a structural deformation, which is reported to be tetragonal.[17]

However, the structure of the magnetic phase of this compound is not fully understood yet. Neutron-scattering experiments have proven that noncollinear commensurate antiferromagnetic order is established below the transition temperature but the details of the magnetic structure are still under heavy debate. It was speculated that a multi-*k* structure is formed.[20,21] Moreover, sample-dependent intensities of the magnetic reflections suggest that $ZnCr_2O_4$ is critically located close to several spin structures.[20]

Magnetic resonance is a convenient tool to study low-energy spin dynamics of the ordered magnets, since it accesses an energy scale unavailable by other techniques (below 0.3 meV). Earlier magnetic resonance studies either were focused on the paramagnetic state[22] or were done on powder samples.[23] The present study fills this gap and reports results of a comprehensive magnetic resonance study in the ordered phase of $ZnCr_2O_4$ done on high-quality single crystals. Our observations indicate the presence of several structural domains in the sample, which can be effectively aligned by field cooling in a moderate magnetic field. We observe several gapped resonance modes. We demonstrate that the observed low-energy spin dynamics can be described assuming a single noncollinear magnetic structure and orthorhombic lattice symmetry in the ordered phase.

II. EXPERIMENTAL DETAILS

$ZnCr_2O_4$ single crystals were grown by chemical transport reactions from polycrystalline starting material prepared by solid-state reactions of stoichiometric binary zinc and chromium oxides of 99.99% purity. Perfect single crystalline samples of octahedral shape and dimensions up to 3 mm on the edge were obtained. X-ray diffraction at room temperature revealed a single-phase material with the cubic spinel structure with a lattice constant $a=8.332(1)$ Å and an oxygen fractional coordinate $x=0.263(1)$. The magnetic properties were studied using a commercial superconducting quantum interference device (SQUID) magnetometer (Quantum Design MPMS-5) working at fields up to 50 kOe.

Magnetic resonance measurements in the wide frequency range from 20 to 150 GHz were performed at the Kapitza Institute. For these measurements we have used a set of home-made transmission-type electron-spin-resonance (ESR) spectrometers equipped with a superconducting cryomagnet. High-sensitivity X-band (9.3 GHz) magnetic resonance experiments were carried out using a Bruker "Elexsys E500" continuous wave spectrometer equipped with an Oxford Instruments helium gas-flow cryostat. Magnetic resonance-absorption spectra were recorded at different frequencies for three principal orientations of the magnetic field: $\mathbf{H}\|\langle 001\rangle,\langle 110\rangle,\langle 111\rangle$. The measurements were mostly

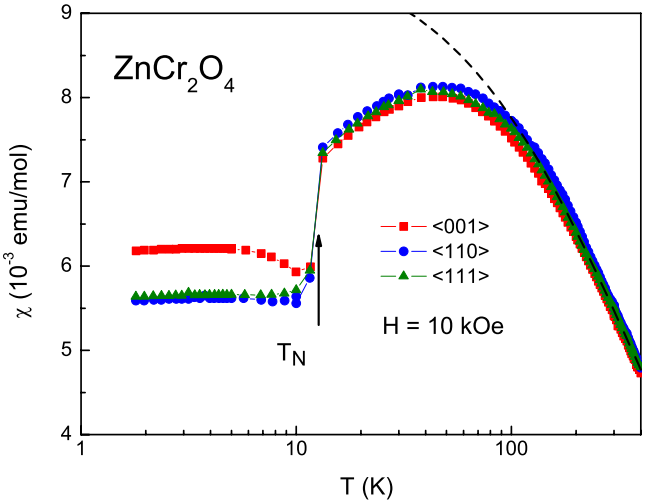

FIG. 1. (Color online) Symbols: temperature dependences of the magnetic susceptibility $\chi = M/H$ in different principal orientations. All curves are measured on cooling in a field of 10 kOe. Dashed curve: high-temperature fit by a Curie-Weiss law with $\Theta = -380$ K.

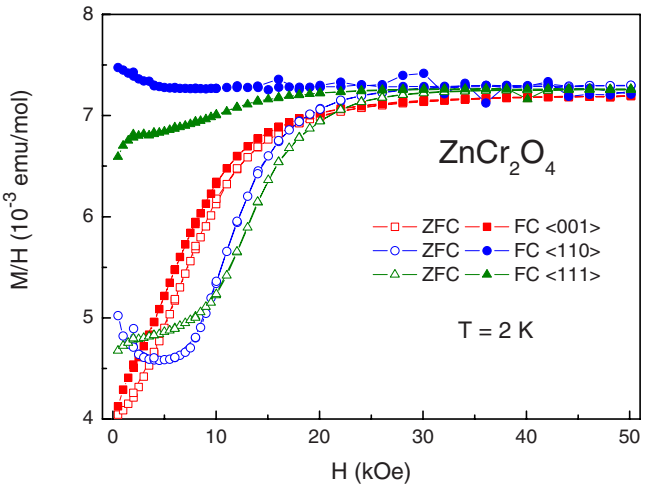

FIG. 2. (Color online) Field dependences of the magnetization divided by field for the ZFC (open symbols) sample and FC (closed symbols) for different orientations at $T = 2$ K.

done on zero-field-cooled samples; the effect of field cooling was checked at certain frequencies.

III. EXPERIMENTAL RESULTS

Figure 1 shows the temperature dependence of the magnetic susceptibility of $ZnCr_2O_4$ single crystals for the magnetic field applied along all three characteristic directions of the cubic system. The susceptibility is isotropic above the AFM transition temperature $T_N = 12.5$ K. At high temperatures the susceptibility follows a Curie-Weiss law but deviates already at about 100 K and develops a broad maximum around 50 K indicative for short-range AFM correlations. At T_N one observes a discontinuous change in the data typical for a first-order transition. In the magnetically ordered regime, the magnetic susceptibility of the zero-field-cooled sample shows a pronounced anisotropy with the highest value for measurements along the $\langle 001 \rangle$ direction (for the measurements in the field of 10 kOe).

To investigate the anisotropy in more detail, the magnetization was measured dependent on the magnetic field both for zero-field cooling (ZFC) as well as after field cooling (FC). As shown in Fig. 2, the ZFC data in all orientations manifest a nonlinear behavior of the magnetization (i.e., $M/H \neq$ const) in fields up to 20 kOe and a linear increase in the magnetization ($M/H =$ const) for higher fields. A nonlinearity of the magnetization in the magnetically ordered state is usually connected to the rotation of the order parameter (as the orientation of the susceptibility tensor of the ordered phase is bound to the order-parameter orientation). The linear increase in the M/H curve for $\mathbf{H} \| \langle 001 \rangle$ indicates a smooth rotation of the order parameter in this orientation. For the two other directions M/H is almost constant below 10 kOe and above 20 kOe, while it changes strongly at around 15 kOe. This change in the susceptibility from a smaller value to a larger one above the critical field is typical for a spin flop. Field cooling was done here in a magnetic field of 50 kOe from above the transition temperature (approximately, from 20 K). It has only a weak effect for $\mathbf{H} \| \langle 001 \rangle$ but leads to nearly constant M/H for the other two orientations. In the field-cooled sample the largest value of magnetic susceptibility is observed for $\mathbf{H} \| \langle 110 \rangle$.

The evolution of the resonance-absorption spectrum with temperature is shown in Fig. 3. At high temperatures (in the paramagnetic phase) a single absorption component with a g factor close to 2.0 is observed. The transition to the antiferromagnetically ordered state is clearly marked by the discontinuous transformation of the resonance-absorption spectrum. Below the Néel temperature T_N, the absorption spectrum consists of several components strongly shifted from the paramagnetic resonance position. No hysteresis exceeding the resolution limit of 0.1 K was detected at the transition. On cooling below T_N the resonance lines first

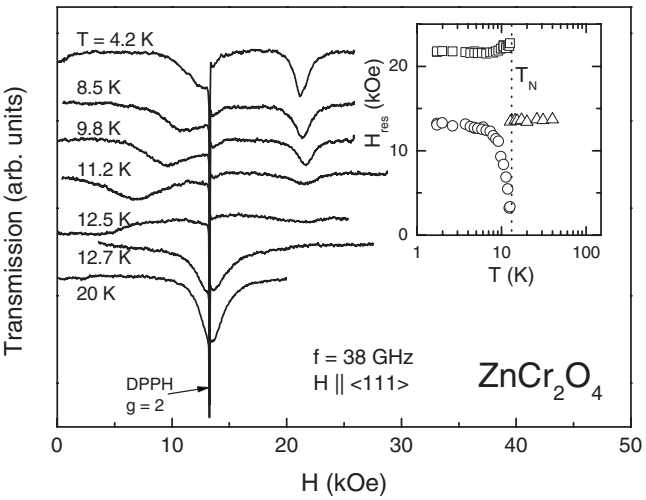

FIG. 3. Field dependences of the microwave absorption at different temperatures (ZFC sample). Inset: temperature dependence of the resonance fields. The narrow line at $H = 13$ kOe is a diphenylpicrylhydrazyl (DPPH) ($g = 2.0$) marker.

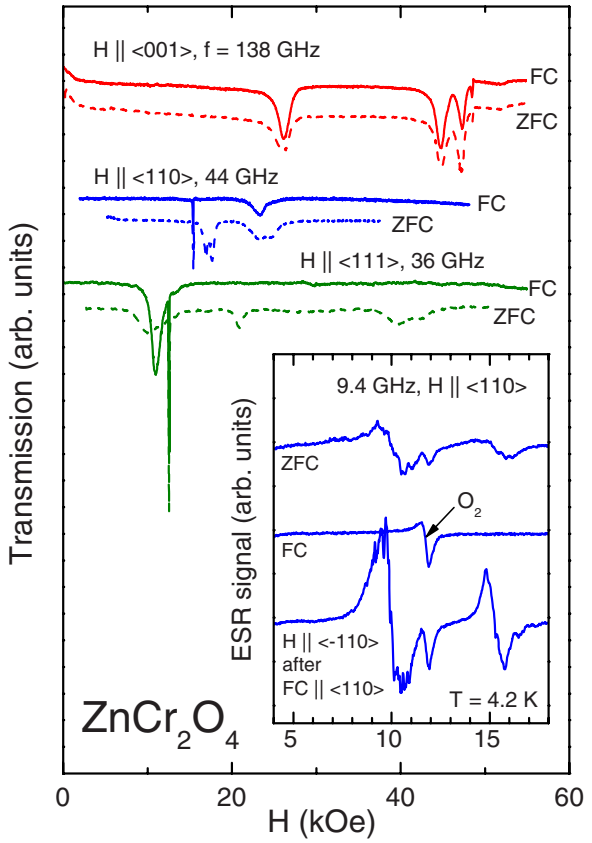

FIG. 4. (Color online) Comparison of the resonance absorption observed at 1.8 K in ZFC and FC samples for different orientations of the magnetic field. Inset: field-cooling effect on the AFM soft mode at $T=4.2$ K and $f=9.4$ GHz. After FC only the background signal remains (due to frozen oxygen).

show a pronounced shift, but below 5 K the temperature dependence of the resonance positions is negligible.

The shape of the resonance-absorption spectra is strongly affected by field cooling. Figure 4 compares the resonance absorption measured on ZFC and FC samples. Here field cooling was performed at a field of 50 kOe starting from 20 K. For $\mathbf{H}\|\langle 110\rangle$ and $\langle 111\rangle$, field cooling leads to the disappearance of some of the absorption components. The remaining absorption components are usually slightly shifted from the corresponding absorption component measured on the ZFC sample. The vanishing absorption intensity does not necessarily add to the remaining components: for example, for $\mathbf{H}\|\langle 110\rangle$, the intensity of the remaining component after field cooling is the same as for the ZFC sample. For $\mathbf{H}\|\langle 001\rangle$ field-cooling effects are less evident—all absorption components are observed in FC samples; field cooling leads only to a slight change in the absorption intensity.

Actually, application of a field of 50 kOe during the cooling seems to be excessive. It is enough to cool the sample at the moderate field of 18 kOe to suppress some of the resonance modes as can be seen in the inset of Fig. 4. Especially, the soft modes indicative for spin reorientation disappear after field cooling but reappear as the sample is rotated to another crystallographically equivalent position. Note that the nonlinearity of the magnetization curve also vanishes after field cooling for $\mathbf{H}\|\langle 110\rangle$.

The stability of the ZFC resonance absorption under prolonged exposure to the magnetic field below T_N was also checked by the high-sensitive X-band measurements. At 4 K the shape of the resonance absorption is reproducible to the finest details. However, at 8 K (which is still below T_N) keeping the $\mathbf{H}\|\langle 110\rangle$-oriented sample at 18 kOe for 90 min leads to 30% reduction in the observed resonance absorption.

The angular dependence of the ESR absorption was measured at 9.3 GHz. As the sample is rotated around the $\langle 001\rangle$ axis (rotation axis perpendicular to the magnetic field), the resonance absorption is observed only in the close vicinity of the $\langle 110\rangle$-like orientations of the applied magnetic field. As the sample is rotated away from these orientations the resonance absorption disappears. This finding indicates directly that $\langle 110\rangle$ is a symmetry chosen direction in the ordered phase.

The entire frequency-field diagrams for the different orientations of the magnetic field are given in Fig. 6. These dependences demonstrate the presence of several resonance modes with zero-field gaps of 21 ± 2 GHz and 113 ± 2 GHz. The higher gap value well corresponds to the data of Ref. 23. For $\mathbf{H}\|\langle 110\rangle$ and $\langle 111\rangle$, one of the resonance modes softens in the magnetic field between 10 and 15 kOe. Note that the nonlinearity of the magnetization curves is also observed in the same field range for these directions (Fig. 2). Field cooling reduces the number of the observed resonance modes to two: one for each of the zero-field gaps.

IV. DISCUSSION

A. Phase transition, domains, and field cooling

As documented above, the change in the resonance field at the phase transition is discontinuous. In conventional molecular-field approximation, the shift of the antiferromagnetic resonance (AFMR) field with respect to the paramagnetic resonance is proportional to the magnitude of the order parameter, i.e., to the sublattice magnetization. The discontinuous change in the resonance field at the phase transition indicates that the order parameter is not small even just below the transition temperature. This observation is in agreement with the first-order nature of the phase transition in $ZnCr_2O_4$.[17,24]

The magnetic susceptibility of the paramagnetic phase is isotropic due to its cubic symmetry. The cubic symmetry is lost in the ordered state because of the lattice deformation. The lattice-strain direction can take one of the equivalent crystallographic axes. The susceptibility tensor of the antiferromagnet is anisotropic, the orientation of its principal axes is determined by the orientation of the order parameter, and the latter is fixed by anisotropic interactions with respect to the crystallographic axes. Therefore, the susceptibility tensors of different structural domains are oriented differently and the gain in the Zeeman energy is different for different domains. Thus, the application of magnetic field makes one of the domains more favorable. It provides an obvious mechanism for the observed field-cooling effect and for the instability of the resonance absorption close to T_N described in Sec. III. This assumption is in agreement with the increase

in the magnetic susceptibility in the field-cooled sample (Fig. 2).

In the case of a cubic-to-tetragonal lattice transition, the formation of the domain structure is well studied for ferroelastic systems. A complicated domain structure consisting of thin twinned domains is usually formed in ferroelastics (see, for example, recent Refs. 25 and 26). Twinning allows to avoid strong local strain at the contact of the domains with different directions of deformation axes. The thickness of twin domains observed in the doped ferroelastic high-temperature superconducting compound $YBa_2Cu_3O_7$ is about 10–100 nm.[26] Twinning also leads to a slight tilting (of the order of $\Delta a/a$) of the domain axes from the corresponding crystallographic axes of the high-temperature phase. While the axes tilting is too small ($\Delta a/a \sim 10^{-3}$) to be of importance, small domain thickness could result in excitation of standing spin waves with $k \sim 1/L$ (L is a domain thickness) instead of a uniform $k=0$ oscillation. This size effect can be a possible reason for the slight shift of the resonance-absorption position in the FC sample marked in Sec. III.

The size effect allows to estimate the thickness of the crystallographic domains. We assume a quadratic spectrum of antiferromagnetic spin waves,

$$E = \sqrt{\Delta_0^2 + \alpha^2 k^2}. \tag{1}$$

Here Δ_0 is the $\mathbf{k}=0$ gap in the spectrum of the antiferromagnetic magnons, $\alpha \sim Ja$ (J denotes the exchange coupling constant between nearest-neighbor spins at distance a), and magnetic field $H=0$. From the magnetic resonance point of view, the energy E in Eq. (1) is the zero-field gap of the AFMR mode. If $\alpha k \ll \Delta_0$, the effective zero-field gap for the standing spin waves is larger than that for the uniform oscillation by $\delta = \alpha^2 k^2/(2\Delta_0)$. Consequently, the resonance branches of the monodomain (FC) sample should be shifted downward (on the H-f plane) by δ with respect to the resonance branches of the multidomain (ZFC) sample: i.e., for the branches rising with the field, the remaining absorption component of the FC sample shifts at the given frequency to higher fields with respect to its position in the case of the ZFC sample. This slight shift is observed in the experiment (Fig. 4); its magnitude does not exceed the half width of the absorption line. We estimate δ/h as 1 GHz (h is the Planck constant). Then, the domain thickness can be estimated as

$$\frac{L}{a} \sim \frac{J}{\sqrt{\Delta_0 \delta}}, \tag{2}$$

which yields [substituting $J/k_B = 20$ K (Ref. 27) and $\Delta_0/h = 20$ GHz] $L/a \sim 100 \gg 1$.

In further discussion, we assume that the domains are thick enough to be considered as bulk antiferromagnet and that the domain walls do not contribute to the magnetic resonance absorption.

B. Application of the exchange-symmetry theory

The theory of exchange symmetry[28] provides a convenient formalism for the analysis of the low-energy dynamics of a magnetically ordered system. This approach allows to describe all symmetry-based low-energy properties of a magnet without considering its detailed microscopic structure or any model assumption. It was successfully applied for different magnets with complicated magnetic structures, e.g., the garnet $Mn_3Al_2Ge_3O_{12}$,[29] the triangular antiferromagnet $CsNiCl_3$,[30] and the rare-earth pyrochlore $Gd_2Ti_2O_7$.[31] It is valid as long as the magnetic-order-parameter structure is determined by the exchange interaction, while the magnetic field and relativistic interactions affect only the orientation of the order parameter but not its structure. Under this assumption, the antiferromagnetic order parameter can be represented by at most three unitary orthogonal antiferromagnetic vectors $\mathbf{l}^{(i)}$ which transform by irreducible representations of the crystal-symmetry group. The number of vectors and these representations define the exchange symmetry of the magnet; e.g., in the simplest case of a collinear antiferromagnet, the order parameter is a single antiferromagnetic vector parallel to the sublattice magnetization. For the case of a noncollinear antiferromagnet the order parameter consists of two (for the planar structure) or three antiferromagnetic vectors. In the following discussion in the case of a planar magnetic structure (i.e., only two vectors), we denote for the sake of simplicity $\mathbf{l}^{(3)} = [\mathbf{l}^{(1)} \times \mathbf{l}^{(2)}]$. The antiferromagnetic vectors $\mathbf{l}^{(i)}$ coincide with the eigenvectors of the susceptibility tensor of the antiferromagnet.

The dynamic equations are derived using a Lagrangian formalism. The kinetic energy of the homogeneous oscillations of a noncollinear antiferromagnet is given by[28]

$$\mathcal{K} = \frac{1}{2\gamma^2} \sum_{\alpha\beta} \chi_{\alpha\beta} (\Omega_\alpha + \gamma H_\alpha)(\Omega_\beta + \gamma H_\beta), \tag{3}$$

where γ is the gyromagnetic ratio of the free electron, $\chi_{\alpha\beta}$ is the susceptibility tensor, and $\mathbf{\Omega}$ is the angular velocity of the order-parameter rotation in the spin space. The kinetic energy can be rewritten via the components of the order parameter and their time derivatives (see Appendix B for details) yielding the Lagrange function,

$$\mathcal{L} = \sum_i \frac{I_i}{2} \left(\dot{\mathbf{l}}^{(i)} - \gamma [\mathbf{l}^{(i)} \times \mathbf{H}] \right)^2 - U_a. \tag{4}$$

Here the constants I_i are related to the susceptibility eigenvalues (see Appendix B) and the term U_a includes small relativistic corrections to the main exchange part due to spin-orbital and dipole-dipole effects. These corrections can be expanded by the components of the antiferromagnetic vectors. The Lagrange function must be invariant under all transformations of the crystallographic symmetry group, which results in some relations between the coefficients in U_a expansion. These relations vary for different exchange-symmetry groups.

The dynamic equations are obtained by taking a variational derivative of the Lagrangian (4) over the rotations of the spin space. These equations should be linearized near the equilibrium position to obtain the eigenfrequencies of small oscillations. In general case, if the magnetic field is not aligned along one of the antiferromagnetic vectors, the equilibrium positions cannot be determined analytically. To model the observed frequency-field dependences, we per-

form numerical calculations of the oscillation eigenfrequencies. We use standard minimization routines to find an equilibrium orientation of the order parameter. This modeling procedure is combined with a fitting algorithm using the constants I_i and the coefficients of the U_a expansion as fit parameters. The static properties are described within the same model and by the same parameters. Knowing the constants I_i and the orientation of the order parameter it is easy to find the susceptibility tensor.

The equilibrium position and eigenfrequencies of the order-parameter precession are insensitive to the simultaneous scaling of the I_i parameters and parameters of the U_a expansion. Thus, to simplify calculations, we locked the I_3 parameter value to 1.00 $\mathrm{kOe}^2/\mathrm{GHz}^2$.

When performing the expansion of the relativistic corrections, it is necessary to take into account that in the case of $ZnCr_2O_4$ the magnetic unit cell is larger than the crystallographic one.[21,32] Therefore some components of the order parameter are not invariant under some of the translational elements of the crystallographic symmetry group. Since the crystal-symmetry group D_{2d}^9 suggested in Ref. 21 has a point symmetry D_{2d} in the vertex of the crystallographic cell, we will focus primarily on the point-symmetry subgroup. Note that this special property remains for all subgroups of D_{2d}^9. Thus, in discussing the lowering of the lattice symmetry below T_N to D_2^7, we will focus primarily on the point-symmetry subgroup.

Although some representations of D_{2d} allow weak ferromagnetism, the susceptibility measurements do not reveal any spontaneous magnetization. This can be either due to the spontaneous magnetization being too small or, more likely, there is no weak ferromagnetism for the exchange group in the present case. Therefore, we will not take weak ferromagnetism into account in further discussion.

C. Evidence for orthorhombic distortions below T_N

Here we will demonstrate that the assumption of the tetragonal lattice symmetry in the ordered phase contradicts the experimental observation described in Sec. III and the explanation of the experimental findings requires a further reduction to orthorhombic symmetry.

First, we note that the symmetry of the magnetic structure below T_N is lower than tetragonal. This statement follows directly from the observation of the distinct field-cooling effect for $\mathbf{H}\|\langle 111\rangle$ since this field orientation is equivalent for all tetragonal domains.

We will characterize each domain by the orientation of the orthogonal basis "*xyz*" with the z axis coinciding with the tetragonal deformation direction (i.e., S_4 axis for the D_{2d} lattice symmetry). By x and y we will denote the directions of the twofold axes perpendicular to the z axis. Since the magnetic symmetry is lower than tetragonal, the x and y directions are not equivalent at least for the magnetic domain.

For the tetragonal lattice deformation only three types of different crystallographic domains, differing by the direction of the tetragonal axis z ($z\|[001],[010],[001]$), can be formed at the transition. Then, two types of magnetic domains with different choice of x and y axes can be formed in each crystallographic domain. To find possible orientations of the x and y axes of each domain, one should consider that the reduction in the point symmetry from O_h to D_{2d} could be done in two ways: (i) by removal of the [100] and [010] symmetry axes as well as (110) and $(1\bar{1}0)$ mirror planes and (ii) by removal of the [110] and $[1\bar{1}0]$ symmetry axes as well as (100) and (010) mirror planes with the former fourfold axes [100] and [010] becoming twofold axes. In the second choice of axes, the magnetic field aligned along the $\langle 111\rangle$ direction would be equivalent for all domains and there would be no reason for the observed field-cooling effects. Thus, the first possibility has to be realized. (Identification[21] of the tetragonal group D_{2d}^9 as $I\bar{4}m2$ also points to the first possibility, while the second case would result in the different choice of axes and would be identified as $F\bar{4}2m$.) Therefore, x and y axes are aligned along the diagonals of the cubic facets.

TABLE I. Classification of the AFM domains with respect to the cubic axes of the paramagnetic phase.

Domain	x	y	z
(a)	[110]	$[\bar{1}10]$	[001]
(b)	$[1\bar{1}0]$	[110]	[001]
(c)	[101]	$[10\bar{1}]$	[010]
(d)	$[\bar{1}01]$	[101]	[010]
(e)	[011]	$[0\bar{1}1]$	[100]
(f)	$[01\bar{1}]$	[011]	[100]

These considerations allow to classify all possible domains by the orientation of their "*xyz*" basis with respect to the cubic axes of the paramagnetic phase as shown in Table I and on Fig. 5. Some of these domains appear to be equivalent in the particular experimental conditions (here $\mathbf{x},\mathbf{y},\mathbf{z}$ are the unit vectors in the corresponding directions; trivial cases are combined),

$$\mathbf{H}\|[001]$$

domains (a) and (b): $\mathbf{H}\|\mathbf{z}$,
domains (c), (d), (e), and (f): $\mathbf{H}\|\mathbf{x}+\mathbf{y}$,

$$\mathbf{H}\|[110]$$

domain (a): $\mathbf{H}\|\mathbf{x}$,
domain (b): $\mathbf{H}\|\mathbf{y}$
domains (c), (f), (d), and (e): $\mathbf{H}\|\frac{\mathbf{x}+y}{\sqrt{2}}+\mathbf{z}$,

$$\mathbf{H}\|[111]$$

domains (a), (c), and (e): $\mathbf{H}\|\sqrt{2}\mathbf{x}+\mathbf{z}$
domains (b), (d), and (f): $\mathbf{H}\|\sqrt{2}\mathbf{y}+\mathbf{z}$.

Note that for the $\mathbf{H}\|\langle 111\rangle$ field orientation, there are only two types of different magnetic domains. As one can see from the experimental data in Fig. 6, we observe five resonance branches in this orientation: two originating from the higher gap, two originating from the lower gap, and one in the high-field–low-frequency part of the frequency-field dia-

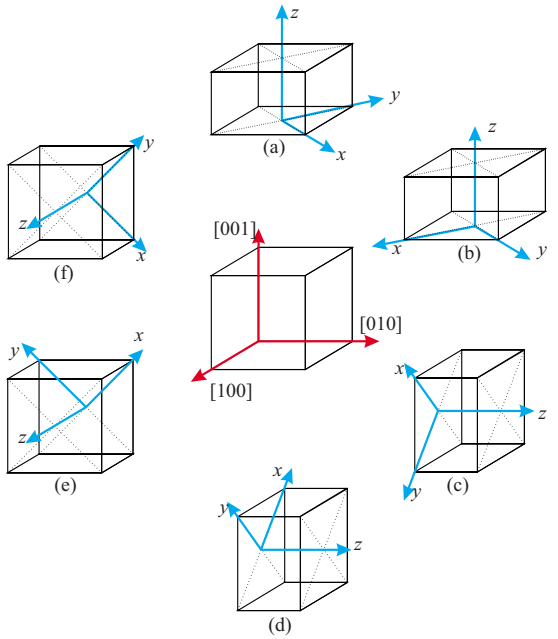

FIG. 5. (Color online) Orientation of the domains' "*xyz*" bases with respect to the cubic axes of the high-temperature unit cell. Tetragonal strain is shown out of scale. [(a)–(f)] Domains enumeration is the same as elsewhere in the text.

gram. The observation of this fifth branch indicates the existence of a third zero-field gap which is not observed directly and is less or equal in magnitude than the lowest-observed gap of 21 GHz.

To apply the exchange-symmetry theory as described in Sec. IV B it is necessary to specify the symmetry of the order parameter. The point-symmetry group D_{2d} has two-dimensional and one-dimensional irreducible representations. If $\mathbf{l}^{(1)}$ and $\mathbf{l}^{(2)}$ transform by a two-dimensional representation then $I_1=I_2$ and the relativistic contribution to the Lagrangian (4) has the form,

$$U_a = \frac{1}{2}A[(l_x^{(1)})^2 + (l_y^{(2)})^2] + B(l_x^{(1)}l_y^{(2)} + l_y^{(1)}l_x^{(2)}) + C(l_x^{(1)}l_y^{(2)} - l_y^{(1)}l_x^{(2)}) + \frac{1}{2}D(l_z^{(3)})^2. \quad (5)$$

If $\mathbf{l}^{(1)}$ and $\mathbf{l}^{(2)}$ transform differently under translations then $B=C=0$. In the other fundamental case, if $\mathbf{l}^{(1)}$ and $\mathbf{l}^{(2)}$ transform by one-dimensional representations, the relativistic contribution reads as

$$U_a = \frac{1}{2}A(l_z^{(1)})^2 + \frac{1}{2}B(l_z^{(2)})^2 + C(l_x^{(1)}l_y^{(2)} - l_y^{(1)}l_x^{(2)}) \quad (6)$$

or

$$U_a = \frac{1}{2}A(l_z^{(1)})^2 + \frac{1}{2}B(l_z^{(2)})^2 + C(l_x^{(1)}l_y^{(2)} + l_y^{(1)}l_x^{(2)}). \quad (7)$$

Depending on the coefficients of the U_a expansion, there are two general possibilities: (i) the $\mathbf{l}^{(i)}$ lie in the (xz) and (yz) planes and (ii) the $\mathbf{l}^{(i)}$ lie in the planes including the z axis and the bisector of the (xy) plane (i.e., in the D_{2d} group mirror planes). $ZnCr_2O_4$ could correspond only to the first case, since in the second case for $\mathbf{H}\|\langle 111\rangle$ the order-parameter vectors $\mathbf{l}^{(1)}$, $\mathbf{l}^{(2)}$, and $\mathbf{l}^{(3)}$ in all magnetic domains

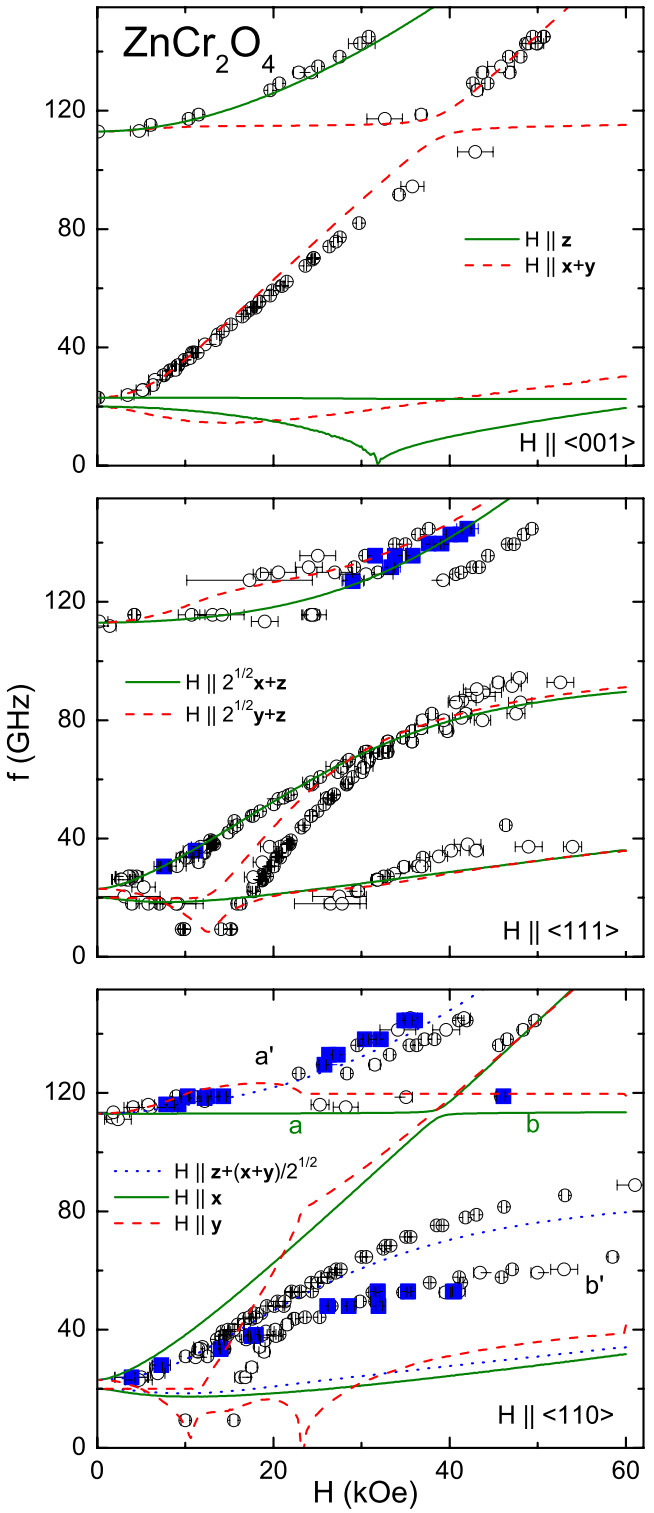

FIG. 6. (Color online) Frequency-field dependences of the resonance modes for the principal cubic orientations (open symbols: ZFC; closed symbols: FC). The numeric calculations (lines) are based on Eq. (9). Fit parameters: see text.

form the same angles with the field direction, which should result in the absence of the field-cooling effects.

We tried to fit the experimentally observed frequency-field dependences applying the exchange-symmetry theory as described above with different forms of U_a [Eqs. (5)–(7)]. However, we did not reach any reasonable agreement of the modeled curves with the experiment. The main problem appearing during numerical modeling is the instability of the domain demonstrating a spin-reorientation transition above the transition field. The reason of this disagreement can be explained qualitatively: namely, it can be proven (see Appendix A) that for the tetragonal D_{2d} lattice symmetry the domain manifesting a spin-reorientation transition becomes indistinguishable from the other domains above the transition field. This is due to the fact that even for a magnetic symmetry lower than tetragonal, the anisotropic contribution U_a reflects the tetragonal crystal symmetry. Thus, after the spin-reorientation transition, the reoriented domain appears to be in a state with the Zeeman energy lower than before reorientation but with the same value of the anisotropic term U_a. The equivalence of the magnetic domains above the transition should provide the same magnetic resonance frequencies above the spin-flop transition. Moreover, there would be no reason for these domains to split again as the magnetic field is reduced to zero. This, however, contradicts the experimental observation of the specific resonance modes corresponding to the domain undergoing a spin reorientation above the spin-flop field, as well as to the reproducibility of the low-field domain structure.

The problem can be solved by the assumption that the lattice deformation at T_N involves not only a compression along the z direction but also a weak in-plane deformation leading to further reduction in the symmetry. The highest symmetry subgroups of D_{2d} are S_4, D_2, and C_{2v}. The S_4 symmetry could be excluded since there are no selected directions in the plane orthogonal to the symmetry axis in this case. Thus the orientation of the order parameter in the (001) plane is arbitrary; it is defined by the interplay of different interactions. This conclusion contradicts to the experimental finding that the ⟨110⟩ orientation is the selected direction. The C_{2v} subgroup could be excluded since in this case selected directions perpendicular to the C_2 axis lie within the mirror planes, i.e., along ⟨100⟩ and ⟨010⟩—which again contradicts to the experimental finding that the ⟨110⟩ orientation is the selected direction. Therefore, our choice is limited to D_2 point symmetry [the corresponding space subgroup of D_{2d}^9 is D_2^7 $(F222)$] with second-order axes along ⟨001⟩ directions (z) and along ⟨110⟩ directions (x and y). This assumption provides inequivalent crystallographic domains differing by the x and y directions. These structural domains can be classified by the orientation of their "xyz" basis in the same way as the magnetic domains. The assumed orthorhombic distortions were not detected in the earlier structural studies,[17,21] most likely because they are smaller than the experimental resolution.

D. Modeling of the static and dynamic properties for the case of orthorhombic distortions

We modeled the antiferromagnetic resonance frequency-field dependences assuming orthorhombic distortions below T_N. As was explained above, to write down the expansion of U_a we will focus again on the point-symmetry group. The D_2 symmetry group has four one-dimensional representations. There are only four fundamentally different cases; the others can be reduced to them by renaming the axes x and y or vectors $\mathbf{l}^{(1)}$ and $\mathbf{l}^{(2)}$,

$$U_a = \frac{A}{2}(l_z^{(1)})^2 + \frac{B}{2}(l_z^{(2)})^2 + \frac{C}{2}(l_x^{(1)})^2 + \frac{D}{2}(l_x^{(2)})^2 + E(l_x^{(1)}l_y^{(2)} - l_y^{(1)}l_x^{(2)}) + F(l_x^{(1)}l_y^{(2)} + l_y^{(1)}l_x^{(2)}), \quad (8)$$

$$U_a = \frac{A}{2}(l_z^{(1)})^2 + \frac{B}{2}(l_z^{(2)})^2 + \frac{C}{2}(l_x^{(1)})^2 + \frac{D}{2}(l_x^{(2)})^2 + E(l_y^{(1)}l_z^{(2)} - l_z^{(1)}l_y^{(2)}) + F(l_y^{(1)}l_z^{(2)} + l_z^{(1)}l_y^{(2)}), \quad (9)$$

$$U_a = \frac{A}{2}(l_z^{(1)})^2 + \frac{B}{2}(l_z^{(2)})^2 + \frac{C}{2}(l_x^{(1)})^2 + \frac{D}{2}(l_x^{(2)})^2 + El_z^{(1)}l_z^{(2)} + Fl_x^{(1)}l_x^{(2)}, \quad (10)$$

$$U_a = \frac{A}{2}(l_z^{(1)})^2 + \frac{B}{2}(l_z^{(2)})^2 + \frac{C}{2}(l_x^{(1)})^2 + \frac{D}{2}(l_x^{(2)})^2. \quad (11)$$

Here we again exclude weak ferromagnetism from the consideration. The choice between Eqs. (8)–(11) is determined by the details of the order-parameter symmetry. In the first case [Eq. (8)] the spin vectors $\mathbf{l}^{(1)}$ and $\mathbf{l}^{(2)}$ transform like $\mathbf{x}$ and $\mathbf{y}$, respectively (or vice versa), while in the second case [Eq. (9)] they transform like $\mathbf{y}$ and $\mathbf{z}$. For both of these cases their transformations under translations should be the same. The next form of energy [Eq. (10)] is feasible if the spin vectors transform by the same one-dimensional irreducible representation of the full crystal-symmetry group. If under some translation the vector $\mathbf{l}^{(1)}$ changes its sign and the vector $\mathbf{l}^{(2)}$ does not, no invariant terms of form $l_\alpha^{(1)}l_\beta^{(2)}$ can be formed which results in the form of energy (11).

The low symmetry of the ordered state results in too many free parameters in the equations of spin dynamics (four to six coefficients in the U_a expansion and two of the three I_i constants). By fixing the zero-field gaps of the AFM resonance spectra, we can put only three analytical constraints on these parameters. Other constraints are expected to appear during the fitting of the modeled AFM resonance spectra. This involves too many degrees of freedom for the assumptions on the sort of equilibrium position, the way the spin-flop transition takes, and the correspondence between structural domains and resonance branches. The reasonable agreement of the modeled curves with the experiment could be obtained for any of the U_a expansions (8)–(10). Namely, the zero-field gaps and spin-reorientation transitions could be reproduced, high-field slopes of different AFM resonance branches could be modeled to the correct values, and crossings and anticrossings of the certain branches could be achieved. Since all these best fits are obtained with essentially nonzero parameters E or F, we are quite confident that the form of U_a given by Eq. (11) is incompatible with the experimental data [since Eq. (11) is, formally, a particular case of the other equations for $E=F=0$]. However, we cannot exclude any of the possi-

bilities described by Eqs. (8)–(10) judging from our results only; one needs additional data on the magnetic structure to select one of these cases. Here we present the results of modeling in the case of U_a taken in the form (9). The parameter values used for the computation of the modeled curves are $\gamma=2.8$ GHz/kOe, $I_1=3.93$ kOe^2/GHz^2, $I_2=0.95$ kOe^2/GHz^2, $I_3=1.00$ kOe^2/GHz^2, $A=66\times10^3$ kOe^2, $B=3.4\times10^3$ kOe^2, $C=-6.2\times10^3$ kOe^2, $D=-5.7\times10^3$ kOe^2, $E=-8.7\times10^3$ kOe^2, and $F=0$. The F parameter was fixed to zero to speed up the fitting procedure; the I_3 constant was locked to 1.00 kOe^2/GHz^2 as described above.

From Fig. 6 one can see that the correspondence of the model and experiment is fairly good. The correct quantity of resonance branches is obtained. The values of the zero-field gaps are in good agreement with the experimental data. For orientations $\mathbf{H}\|\langle110\rangle$ and $\langle111\rangle$, the spin-reorientation transitions of certain domains are well reproduced. This modeling indicates that the frequency-field dependences can be reasonably reproduced assuming a single type of order parameter and taking into account all possible domains. There are really just two types of discrepancies between the experimental data and modeled curves: first, there are predicted low-frequency modes at high fields which are not observed; second, for the orientation $\mathbf{H}\|\langle110\rangle$ the modes corresponding to the domain with lowest energy ($\mathbf{H}\|x$) are far from the experimental data corresponding to the domain stable under field cooling (see the fit curves and experimental data marked by a, a', b, and b' in the lower panel of Fig. 6). These discrepancies can be due to the following reasons. In the ESR experiments at 9 GHz, fields up to only 18 kOe were available, whereas above 18 GHz the frequency-field dependences of the low-frequency modes in question are rather flat. In the case of $I_2=I_3$, they become field independent which results in a strong broadening of the resonance modes in the experiments at fixed frequency. Thus, these modes cannot be detected in a field scan. Concerning the discrepancy for the $\mathbf{H}\|x$ domain, note that the modeled curves still demonstrate an "anticrossing." This feature, probably, can be enhanced by varying the parameter sets (for we cannot exclude that we did not miss some prominent areas of the parameter space during numerical search for the best fit) or by higher-order terms in the energy expansion.

We also modeled static magnetic properties with the same set of parameters. The results of this modeling are shown in Fig. 7. This modeling demonstrates that the spin-reorientation transition is realized by a continuous rotation of the order parameter as shown, e.g., for the y domain in the inset of Fig. 7. This explains the absence of a sharp change in the magnetization at the spin-reorientation transition. The field dependence of the magnetization is qualitatively well reproduced. It demonstrates a nonlinear behavior with a characteristic change during the spin reorientation for the unfavorable domains (see top panel of Fig. 7), which disappear after field cooling, and an almost linear behavior for the favorable domains which remain after field cooling. The energy difference between different domains shown in the upper frame of this figure explains the observed field-cooling phenomena. The domains corresponding to the modes surviving the field cooling have the lowest energy in the magnetic field. For the orientation $\mathbf{H}\|\langle111\rangle$ the calculated energy difference between the domains is similar and, thus, the field-cooling effect is comparable to the case $\mathbf{H}\|\langle110\rangle$. For $\mathbf{H}\|\langle001\rangle$, this difference is much smaller which can probably explain the much weaker field-cooling effect for this direc-

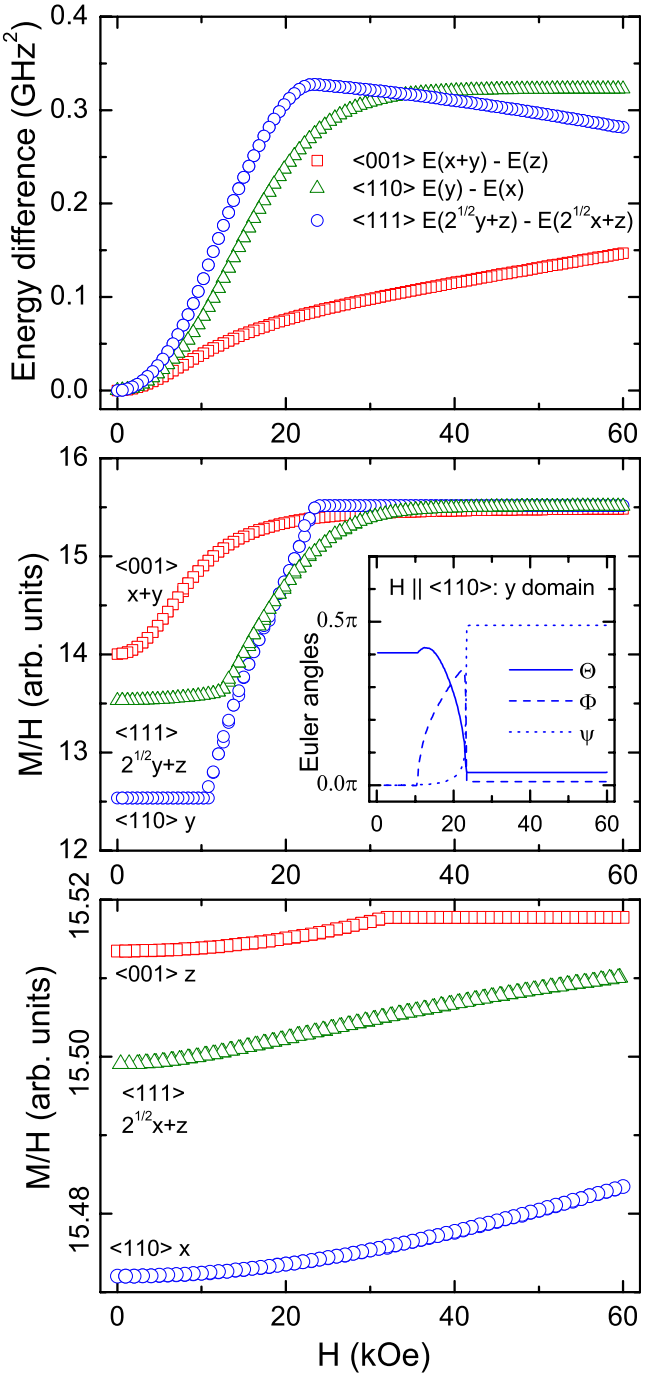

FIG. 7. (Color online) Upper frame: calculated field dependences of the energy difference for various domains. The calculations are done for the same parameters as used for the AFM resonance spectrum shown in Fig. 6. Middle frame: calculated magnetization of the domains with unfavorable orientation. Inset: calculated field dependences of the Euler angles for the $\mathbf{H}\|\langle110\rangle$ y domain. Lower frame: calculated magnetization of the domains with favorable orientation of the order parameter.

tion. However, we have to admit the problem in reproducing the experimentally observed anisotropy of the field-cooled magnetization at low fields. The experimentally highest susceptibility for the monodomain FC sample is observed for $\mathbf{H}\|\langle 110\rangle$ (Fig. 2), while the modeled curves for the presented parameter set indicate a slightly higher susceptibility for the most favorable domain in the $\mathbf{H}\|\langle 100\rangle$ orientation (Fig. 7). Note that the modeled difference of the three favorable domains is tiny; thus for low fields some weak effects related to shape anisotropy or surface effects may destroy the stability of the uniform magnetization.

Summarizing the results of our modeling, we conclude that the low-energy dynamics and static properties of the ordered phase of $ZnCr_2O_4$ can be described by the assumption of a *single* type of magnetic order and of the *orthorhombic* lattice distortions below T_N. This puts a question mark on the possibility to realize different spin structures in $ZnCr_2O_4$ as suggested earlier.[20] We suppose that the complications in the determination of the magnetic structure of $ZnCr_2O_4$ by neutron scattering were caused by the unaccounted orthorhombic deformations and effects of multiple domains.

V. CONCLUSIONS

We have performed a detailed study of the low-energy dynamics of the ordered phase of the frustrated antiferromagnetic spinel $ZnCr_2O_4$. We have proven directly that multiple domains exist below the transition temperature T_N. We have demonstrated that some of these domains are effectively suppressed by field cooling. Spin-reorientation transitions indicated by softening of certain antiferromagnetic resonance modes and by nonlinear behavior of the magnetization are observed.

These results are incompatible with the earlier proposed symmetry of the distorted lattice. Thus, we conclude that the lattice deformation at the phase transition involves small in-plane distortions besides the tetragonal distortions. We suggest that the actual symmetry of the lattice below T_N corresponds to the orthorhombic D_2^7 symmetry.

We have demonstrated that the low-energy dynamics can be reasonably described within the framework of the exchange-symmetry theory, assuming a noncollinear magnetic ordering characterized by a single order parameter.

ACKNOWLEDGMENTS

The authors thank A. I. Smirnov, S. S. Sosin, V. I. Marchenko, L. E. Svistov, and I. N. Khliustikov for the continuous interest and numerous discussions. This work was supported by the RFBR under Grant No. 07-02-00725, by the Russian Science Support Foundation, Russian Presidential Grant for the Young Scientists under Grant No. MK-4569.2008.2, Russian Presidential Grants for the Support of Scientific Schools under Grants No. 6122.2008.2 and No. 3526.2008.2, and partially supported by the Deutsche Forschungsgemeinschaft (DFG) within the collaborative research center under Grant No. SFB 484 (Augsburg).

APPENDIX A: INSTABILITY OF CERTAIN DOMAINS IN CASE OF TETRAGONAL LATTICE SYMMETRY

Here we will prove that for the D_{2d} point symmetry at the spin-reorientation transition, the domain demonstrating this transition becomes indistinguishable from the other domains.

First we consider the case when $\mathbf{l}^{(1)}$ and $\mathbf{l}^{(2)}$ transform by two-dimensional representation of D_{2d}. Minimizing the energy (5) we get the orientation of the order parameter in the absence of magnetic field. For $|B|>|A|$ the solution consists of vectors lying in the mirror planes, which is not the case of $ZnCr_2O_4$ (see above). For $|A|>|B|$ and $A<0$ the two solutions are $\mathbf{l}^{(1)}\|\mathbf{x}$ and $\mathbf{l}^{(2)}$ lying in the (yz) plane and $\mathbf{l}^{(2)}\|\mathbf{y}$ and $\mathbf{l}^{(1)}$ lying in the (xz) plane. The case of $A>0$ can be reduced to this one by renaming the axes x and y. These solutions define two different magnetic domains. If the susceptibility along $\mathbf{l}^{(3)}$ is less than along $\mathbf{l}^{(1)}$ and $\mathbf{l}^{(2)}$ then for $H\|\mathbf{x}$ one of the domains is already in its minimum of the Zeeman energy. The other one is not in the minimum and at some value of magnetic field it will undergo a spin-reorientation transition. As it turns out, there is only one possible state for it after the transition, the same as for the first domain. So after the spin flop these two domains will be indistinguishable. If the susceptibility along $\mathbf{l}^{(1)}$ and $\mathbf{l}^{(2)}$ is less than along $\mathbf{l}^{(3)}$, both domains are not in the minimum of the Zeeman energy when the field is applied along the x axis. After the spin flop, both domains again become indistinguishable.

Now we consider the case when $\mathbf{l}^{(1)}$ and $\mathbf{l}^{(2)}$ transform by one-dimensional representations of D_{2d}. To define the orientation of the order parameter, we minimize the energy (6). We get the result that one of the vectors (let it be $\mathbf{l}^{(1)}$) is aligned in the (xy) plane, but its orientation in this plane remains arbitrary. To find a solution, it is necessary to take into account the next-order terms in the U_a expansion. There is no need to write down all of them; just note that due to the tetragonal symmetry the dependence of U_a on the angle ϕ between $\mathbf{l}^{(1)}$ and $\mathbf{x}$ is $F\cos(4\phi)$. There are two sets of solutions depending on the sign of F. For $F>0$ the solutions are $\phi=\pi/4,3\pi/4,5\pi/4,7\pi/4$, i.e., $\mathbf{l}^{(1)}$ lies in the mirror plane, which is not the case of $ZnCr_2O_4$. For $F<0$ the solutions are $\phi=0,\pi/2,\pi,3\pi/2$. These solutions define two magnetic domains: for one of them $\mathbf{l}^{(1)}\|\mathbf{x}$ and for the other $\mathbf{l}^{(1)}\|\mathbf{y}$. First, no matter along which $\mathbf{l}^{(i)}$ the susceptibility is largest, a spin-reorientation transition is expected for $\mathbf{H}\|(\mathbf{x}\pm\mathbf{y})$ (i.e., $\mathbf{H}\|\langle 001\rangle$). This spin reorientation is either rotation of the order parameter around the z axis by $\pi/4$ or, in the special case of the largest susceptibility being along the z axis, rotation of the largest susceptibility direction to the (xy) plane. However, such a transition is not observed in our experiments. Second, the spin-flop transition observed at $\mathbf{H}\|\langle 111\rangle$ can be caused only by rotation of the order parameter around the z axis, but after this rotation both domains become indistinguishable.

APPENDIX B: DEDUCTION OF THE KINETIC-ENERGY EXPRESSION

First, since eigenvectors of the susceptibility tensor $\chi_{\alpha\beta}$ coincide with the antiferromagnetic vectors $\mathbf{l}^{(1,2,3)}$, one can rewrite,

$$\frac{\chi_{\alpha\beta}}{\gamma^2} = (I_2 + I_3) l_\alpha^{(1)} l_\beta^{(1)} + (I_1 + I_3) l_\alpha^{(2)} l_\beta^{(2)} + (I_1 + I_2) l_\alpha^{(3)} l_\beta^{(3)}$$

$$= \sum_i I_i (\delta_{\alpha\beta} - l_\alpha^{(i)} l_\beta^{(i)}). \quad \text{(B1)}$$

Here $I_1 = (-\chi_1 + \chi_2 + \chi_3)/(2\gamma^2)$, $I_2 = (\chi_1 - \chi_2 + \chi_3)/(2\gamma^2)$, and $I_3 = (\chi_1 + \chi_2 - \chi_3)/(2\gamma^2)$, $\chi_{1,2,3}$ are the susceptibilities along $\mathbf{l}^{(1,2,3)}$, correspondingly, γ is a gyromagnetic ratio.

Then, expressing the time derivative $\dot{\mathbf{l}}^{(i)}$ via the angular velocity $\mathbf{\Omega}$ and using the fact that $\mathbf{l}^{(i)}$ are unitary vectors, one can write down the following equalities:

$$\dot{\mathbf{l}}^{(i)} = [\mathbf{\Omega} \times \mathbf{l}^{(i)}], \quad \text{(B2)}$$

$$\left(\dot{\mathbf{l}}^{(i)}\right)^2 = \mathbf{\Omega}^2 - (\mathbf{\Omega} \cdot \mathbf{l}^{(i)})^2, \quad \text{(B3)}$$

$$\left[\mathbf{l}^{(i)}, \dot{\mathbf{l}}^{(i)}\right] = \mathbf{\Omega} - \mathbf{l}^{(i)} (\mathbf{\Omega} \cdot \mathbf{l}^{(i)}). \quad \text{(B4)}$$

Directly substituting Eqs. (B1)–(B4), one can straightforwardly prove that

$$\sum_i \frac{I_i}{2} \left(\dot{\mathbf{l}}^{(i)} - \gamma [\mathbf{l}^{(i)} \times \mathbf{H}]\right)^2 = \frac{1}{2\gamma^2} \sum_{\alpha\beta} \chi_{\alpha\beta} (\Omega_\alpha + \gamma H_\alpha)(\Omega_\beta + \gamma H_\beta). \quad \text{(B5)}$$

[1] D. J. Huang, C. F. Chang, H.-T. Jeng, G. Y. Guo, H.-J. Lin, W. B. Wu, H. C. Ku, A. Fujimori, Y. Takahashi, and C. T. Chen, Phys. Rev. Lett. **93**, 077204 (2004).

[2] I. Leonov, A. N. Yaresko, V. N. Antonov, M. A. Korotin, and V. I. Anisimov, Phys. Rev. Lett. **93**, 146404 (2004).

[3] S. Kondo, D. C. Johnston, C. A. Swenson, F. Borsa, A. V. Mahajan, L. L. Miller, T. Gu, A. I. Goldman, M. B. Maple, D. A. Gajewski, E. J. Freeman, N. R. Dilley, R. P. Dickey, J. Merrin, K. Kojima, G. M. Luke, Y. J. Uemura, O. Chmaissem, and J. D. Jorgensen, Phys. Rev. Lett. **78**, 3729 (1997).

[4] A. Krimmel, A. Loidl, M. Klemm, S. Horn, and H. Schober, Phys. Rev. Lett. **82**, 2919 (1999).

[5] A. P. Ramirez, R. J. Cava, and J. Krajewski, Nature (London) **386**, 156 (1997).

[6] V. Fritsch, J. Deisenhofer, R. Fichtl, J. Hemberger, H.-A. Krug von Nidda, M. Mücksch, M. Nicklas, D. Samusi, J. D. Thompson, R. Tidecks, V. Tsurkan, and A. Loidl, Phys. Rev. B **67**, 144419 (2003).

[7] K. Ohgushi, T. Ogasawara, Y. Okimoto, S. Miyasaka, and Y. Tokura, Phys. Rev. B **72**, 155114 (2005).

[8] R. Fichtl, V. Tsurkan, P. Lunkenheimer, J. Hemberger, V. Fritsch, H.-A. Krug von Nidda, E.-W. Scheidt, and A. Loidl, Phys. Rev. Lett. **94**, 027601 (2005).

[9] V. Fritsch, J. Hemberger, N. Büttgen, E.-W. Scheidt, H.-A. Krug von Nidda, A. Loidl, and V. Tsurkan, Phys. Rev. Lett. **92**, 116401 (2004).

[10] J. Hemberger, P. Lunkenheimer, R. Fichtl, H.-A. Krug von Nidda, V. Tsurkan, and A. Loidl, Nature (London) **434**, 364 (2005).

[11] S. Weber, P. Lunkenheimer, R. Fichtl, J. Hemberger, V. Tsurkan, and A. Loidl, Phys. Rev. Lett. **96**, 157202 (2006).

[12] J. Hemberger, H. A. Krug von Nidda, V. Tsurkan, and A. Loidl, Phys. Rev. Lett. **98**, 147203 (2007).

[13] J. Hemberger, T. Rudolf, H.-A. Krug von Nidda, F. Mayr, A. Pimenov, V. Tsurkan, and A. Loidl, Phys. Rev. Lett. **97**, 087204 (2006).

[14] T. Rudolf, C. Kant, F. Mayr, J. Hemberger, V. Tsurkan, and A. Loidl, Phys. Rev. B **75**, 052410 (2007).

[15] P. G. Radaelli, Y. Horibe, M. J. Gutmann, H. Ishibashi, C. H. Chen, R. M. Ibberson, Y. Koyama, Y. S. Hor, V. Kiryukhin, and S. W. Cheong, Nature (London) **416**, 155 (2002).

[16] M. Schmidt, W. Ratcliff, P. G. Radaelli, K. Refson, N. M. Harrison, and S. W. Cheong Phys. Rev. Lett. **92**, 056402 (2004).

[17] S.-H. Lee, C. Broholm, T. H. Kim, W. Ratcliff II, and S.-W. Cheong, Phys. Rev. Lett. **84**, 3718 (2000).

[18] O. Tchernyshyov, R. Moessner, and S. L. Sondhi, Phys. Rev. Lett. **88**, 067203 (2002).

[19] O. Tchernyshyov, R. Moessner, and S. L. Sondhi, Phys. Rev. B **66**, 064403 (2002).

[20] J.-H. Chung, M. Matsuda, S.-H. Lee, K. Kakurai, H. Ueda, T. J. Sato, H. Takagi, K.-P. Hong, and S. Park, Phys. Rev. Lett. **95**, 247204 (2005).

[21] S. H. Lee, G. Gasparovich, C. Broholm, M. Matsuda, J.-H. Chung, Y. J. Kim, H. Ueda, G. Xu, P. Zschak, K. Kakurai, H. Takagi, W. Ratcliff II, T. H. Kim, and S. W. Cheong, J. Phys.: Condens. Matter **19**, 145259 (2007).

[22] H. Martinho, N. O. Moreno, J. A. Sanjurjo, C. Rettori, A. J. Garcia-Adeva, D. L. Huber, S. B. Oseroff, W. Ratcliff, S. W. Cheong, P. G. Pagliuso, J. L. Sarrao, and G. B. Martins, Phys. Rev. B **64**, 024408 (2001).

[23] H. Ohta, S. Okubo, H. Kikuchi, and S. Ono, Can. J. Phys. **79**, 1387 (2001).

[24] R. Plumier, M. Lecomte, and M. Sougi, J. Phys. (France) Lett. **38**, L149 (1977).

[25] A. E. Jacobs, S. H. Curnoe, and R. C. Desai, Phys. Rev. B **68**, 224104 (2003).

[26] E. K. H. Salje, S. A. Hayward, and W. T. Lee, Acta Crystallogr., Sect. A: Found. Crystallogr. **61**, 3 (2005).

[27] A. J. García-Adeva and D. L. Huber, Phys. Rev. Lett. **85**, 4598 (2000).

[28] A. F. Andreev and V. I. Marchenko, Sov. Phys. Usp. **130**, 39 (1980).

[29] L. A. Prozorova, V. I. Marchenko, and Yu. V. Krasnyak, JETP Lett. **41**, 637 (1985).

[30] I. A. Zaliznyak, V. I. Marchenko, S. V. Peterov, L. A. Prozorova, and A. V. Chubukov, JETP Lett. **47**, 211 (1988).

[31] S. S. Sosin, A. I. Smirnov, L. A. Prozorova, G. Balakrishnan, and M. E. Zhitomirsky, Phys. Rev. B **73**, 212402 (2006).

[32] A. Olés, J. Phys. Colloq. **32**, C1-328 (1971).